INTERNAL SPATIAL MODES AND LOCAL PROPAGATION PROPERTIES IN OPTICAL WAVEGUIDES MEASURED USING NEAR-FIELD SCANNING OPTICAL MICROSCOPY

BENNETT B GOLDBERG, M. SELIM ÜNLÜ, and GREG VANDER RHODES
Boston University Physics Department, Department of Electrical and Computer Engineering, and Photonics Center, Boston, MA 02215, goldberg@bu.edu

ABSTRACT

Near-field scanning optical microscopy has been used to measure the internal spatial modes and local properties controlling optical wave propagation in glass/silica buried waveguides. The period of the observed standing modes provides a direct measure of the effective index, which combined with the measured transverse modal shape and decay constants, determines the values of all spatial components of the wave vector.

Typically, small fluctuations in the material properties of structures can prevent proper operation as well as accurate diagnostic device modeling. The NSOM local probe measurements provide a means of detailed characterization, and defects in processing and their affects on performance are readily identified. We have also developed a technique that can obtain information about the locations of remote dielectric interfaces based upon the rate of change in the phase of the standing wave as a function of wavelength. Finally, experimental results addressing the issue of perturbation of the NSOM probe on the measurement of the local field shows a weak but measurable perturbation, and the dependence on aperture and material parameters will be discussed.

INTRODUCTION

Optical guided-wave devices are crucial for routing and control applications in the areas of optical communications and networking. As greater bandwidth requirements have pushed performance demands, guided-wave devices have become increasingly more complex. Increased functionality has been achieved through techniques such as evanescent coupling and resonances in microstructures, effects that strongly depend on local field and propagation properties of the waveguides [1]. While accurate simulations of complicated guided-wave devices rely on assumptions about the physical structure, direct measurement of internal optical modes and the local properties of guided-wave propagation have remained elusive.

By using a local probe technique, Near-Field Scanning Optical Microscopy (NSOM) [2-4] , the local evanescent field above the waveguide can be measured, providing a detailed and complete picture of the operation of the guided mode, far surpassing previous indirect imaging techniques [5-8]. NSOM studies of wave-guides have demonstrated evanescent field decay [9], standing modes [10], and recently observed a modulation in the propagation direction [11] due to the Tien effect [12]. To the best of our knowledge, our measurements provide

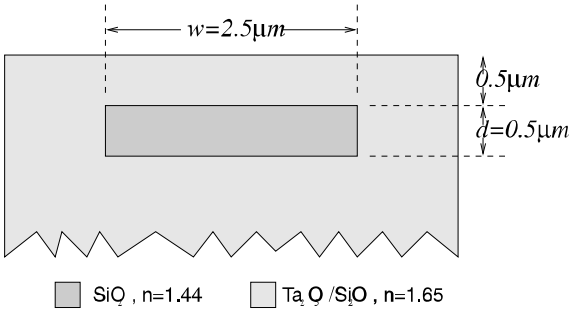

Fig. 1 Schematic of the device under study.

the first observation of standing modes in a single mode waveguide, as well as the first determination of all components of the propagation vector [13].

EXPERIMENTAL SETUP AND DEVICE UNDER STUDY

In Fig. 1, we show a schematic of the waveguide studied. It was fabricated using the traditional sputtering and optical lithographic methods [14,15]. The rectangular core region is composed of a compound Ta_2O_5 / SiO_2 glass of index of n=1.65. The cladding region is pure silica, SiO_2, n=1.44.

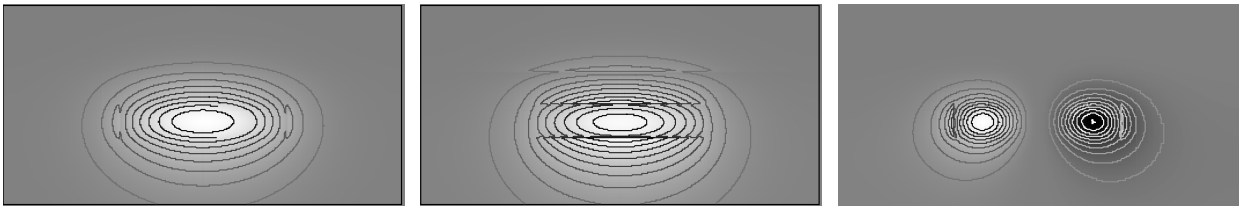

Fig 2: BPM mode simulations of the allowed modes of the glass/silica rectangular waveguide.

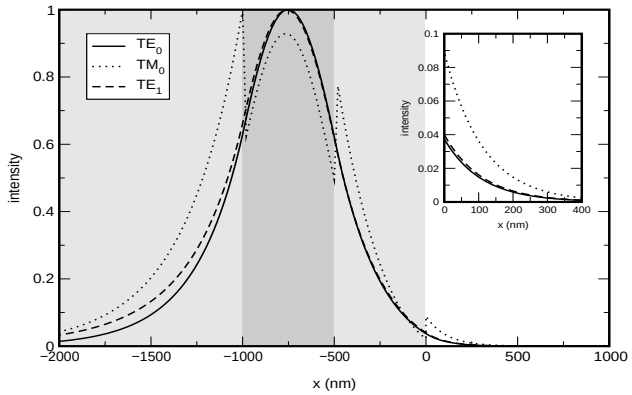

Fig. 3 Vertical line cuts of mode simulations for the three modes guided by the device under test.

We have simulated the mode patterns for this waveguide that are displayed in cross-section in Fig. 2. From a linecut of the intensity of these simulations in the vertical or *x*-direction (Fig. 3), we can see that this waveguide is ideal for an NSOM measurement, due to the relatively large field penetration into the air region. The field intensity at the air interface is about between 4% and 9% that of the maximum in the core region.

The waveguides studied are designed for operation at the telecommunication wavelengths around 1.55 μm. A schematic of the experimental configuration is displayed in Fgi. 4. A tunable external cavity laser (HP 8168F) was used as the light source, tunable from 1440nm to 1570nm. A conically lensed fiber is used to launch this light into the waveguide. Polarization control is performed using polarization paddles.

Transmitted light at the exit facet is imaged onto both a CCD for optimization of

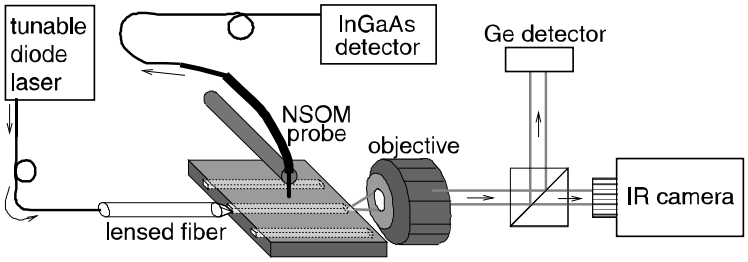

Fig 4 Experimental setup used for characterizing internal optical fields inside guided-wave devices. Light from tunable laser is launched into the device under test, and the transmitted light is analyzed. The NSOM probe is scanned over the surface of the device, measuring both topography and sampling the evanescent field.

coupling and a Ge photodiode for quantitative measurements. A polarizer can be placed before these detectors, so that the desired output polarization can be chosen with the polarization paddles. The NSOM probe is scanned over the surface of the waveguide, routing the collected light to an InGaAs photodetector. The translation stage used to scan the tip is interferometrically calibrated to $\pm 0.3nm$, and a shear-force tuning fork method [16] is used during surface scans to maintain a tip-surface separation of 10 nm.

NSOM MEASUREMENTS

The field at the waveguide surface will not be simply related to the internal modes if a large amount of scattering is present. Therefore, a vital initial measurement in this and similar studies is a comparison of the level of scattered light to that of evanescent field at the surface [13]. The measured optical intensity from NSOM scans in the vertical plane, perpendicular to the direction of light propagation, is plotted in Fig. 5(a) on top of the schematic of the structure. The intensity decays quickly as a function of height showing the absence of scattering into free-space propagating modes. This scan also shows excellent qualitative agreement with the top section of the mode solver simulation, shown in Fig 5(b). A vertical line cut of this data, shown in Fig. 6, exhibits pure exponential behavior consistent with theoretical predictions. We see complete exponential decay until the noise floor of our system is encountered, at about 600nm.

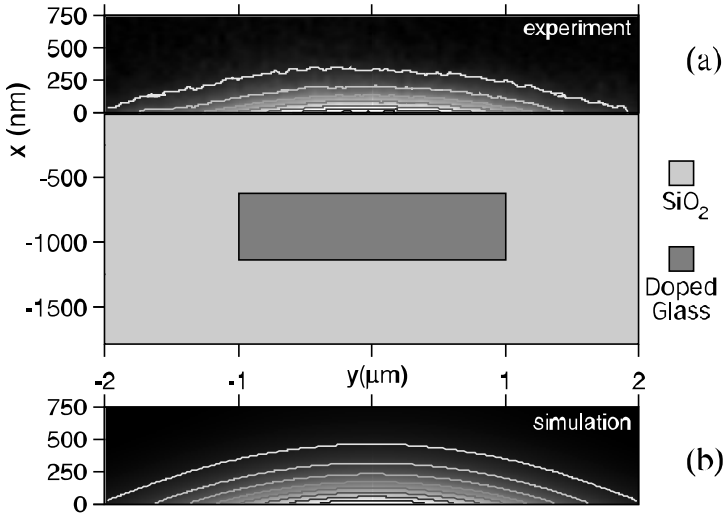

Fig 5 (a) Measured optical intensity from NSOM scans in the vertical plane, shown on top of a cross section of the waveguides under study. Grayscale map uses black to indicate zero intensity, and white for high intensity. Contours are added to enhance visibility of features. A complete decay of the field at a height (x) of around 500nm is observed. (b) Simulation of mode intensity in the same region

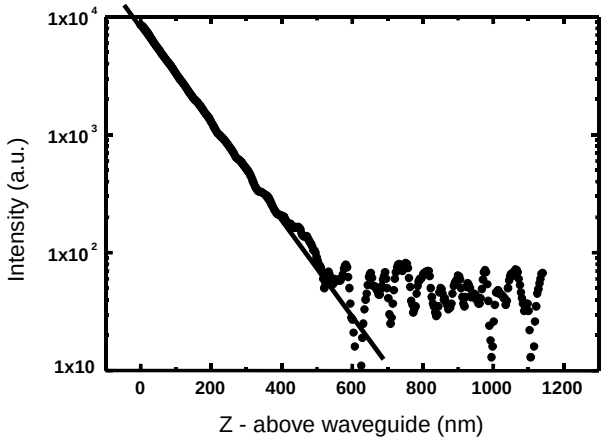

Fig 6 Line cut of Fig. 6(a) at $y=0$, with exponential fit with intensity decay coefficient $\alpha \quad \mu^{-1}$

The buried waveguide design is intended to have a smooth top surface without significant height variation. However, due to the fabrication process a slight ridge on the surface above the buried waveguide is observed, shown in Fig. 7a, allowing us to spatially anchor our optical scans. The actual width of the surface structure does not directly correspond to the buried waveguide dimension since the ridge may not propagate vertically as the top cladding

layer is grown.

A large variation with polarization is observed in the NSOM optical scans, because the measured waveguides are not designed for polarization insensitive operation. When TM modes are excited by controlling the input polarization, we obtain the image shown in Fig.7 (b). The dependence along $\hat{y}$ of the measured optical intensity is consistent with a single mode waveguide. The periodic variation in the $\hat{z}$ direction is the standing wave due to the cavity formed between the entrance and exit facets of the waveguide. The peak-to-valley ratio along is $\hat{z}$ 1.2, consistent with the entrance and exit facet reflectivities, estimated at 4%. The period of the standing mode is given by $\lambda_0/2n_{eff}$, where λ_0 is the vacuum wavelength and n_{eff} is the effective index for the guided optical mode. At $\lambda_0 = 1.549\mu m$, the measured $n_{eff} = 1.458$ compares very favorably with simulations which yield $n_{eff}= 1.473$. Since our scanning stages are interferometrically calibrated the small difference between data and simulation actually provides a more accurate measure of the waveguide dimensions than those initially supplied by the fabricators and used in the simulation.

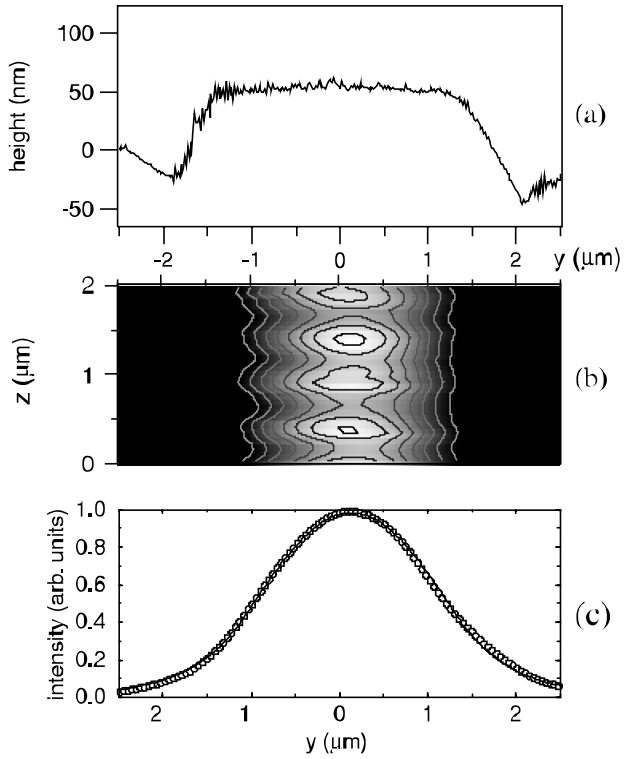

Fig 7: (a) Line-scan of the surface topography across the waveguide, showing ridge at surface due to buried waveguide. (b) Optical image obtained at the surface of the waveguide when TM modes are excited. The periodic variation in the *z* direction is a standing mode due to a cavity formed in the waveguide. A line cut for *y*=0 exhibits almost pure sinusoidal behavior, with a peak-to-valley ratio of 1.2. (c) Line-cut for constant *z*, with a fit to the lowest order solution in a step-index waveguide.

α VARIATION

The traditional method of solving a rectangular waveguide assumes that the values of the components of ***k***, the wave vector, are constant within a region [18]. This assumption, while convenient, leads to unphysical situations, especially at the corners of a rectangular waveguide [19]. In reality, only the component along the propagation direction, k_z is constant everywhere in order to satisfy phase-matching, while k_x and k_y may vary as long as the dispersion relationship is satisfied: $k_x^2 + k_y^2 + k_z^2 = n^2 k_0^2$, for a material with index *n*. Along the direction perpendicular to the waveguide surface $\hat{x}$, the propagation constant is imaginary resulting in an evanescent field $k_x \rightarrow \alpha_x$. Vertical linecuts of Fig. 6 can be fitted to obtain a reduced value of α as a function of *y*, across the waveguide.

OBTAINING k_y

The component of the wavevector ***k*** across the waveguide in $\hat{y}$ can be obtained from the mode shape. The solutions of a step index waveguide give cos $k_y y$ (even order) or sin $k_y y$ (odd order) within the core region, with decaying exponentials outside this region. Fig. 7(c) shows a line cut of the NSOM data long the *y* direction, with a fit to the lowest order solution. The parameters of this fit give k_y and thus k_x in the five regions shown in Fig. 8, with extinction coefficients shown as α_{xy}. The values for k_x and k_y are within 6% of the theoretical predictions shown in parentheses. The values of are in almost perfect agreement with simulation.

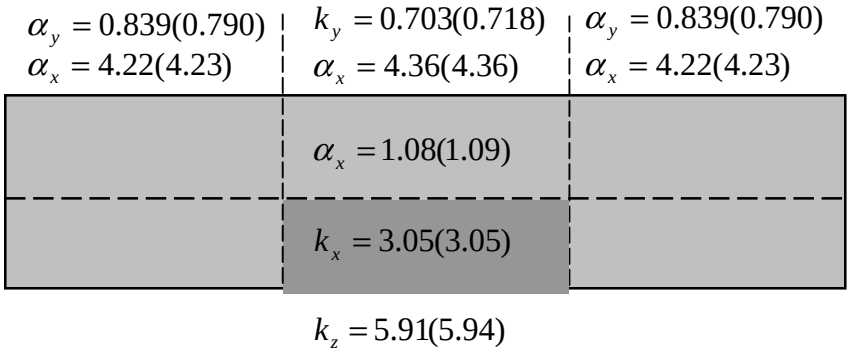

Fig 8: Measured propagation constants in different regions of the waveguide, all in units of μm^{-1}. Simulated quantities are shown in parentheses.

If we take our measured quantities for α_x, k_y, and k_z and insert them into the equation $k_x^2 + k_y^2 + k_z^2 = n^2 k_0^2$ we should naturally obtain k_0. This is a measure of the internal consistency of our measurement technique. The value obtained is $k_0 = 3.894 \mu m^{-1}$, which we can compare to the real value of $k_0 = 4.056\ \mu m^{-1}$. You can make this difference more intuitively physical by finding what index air would have to be to compensate for this difference. Taking the square root of the ratio of these two, we get a value n=1.002. This agreement, while not perfect, may be due to a slight miscalibration of one of the axes used for measuring the period of the standing modes.

TE MODES

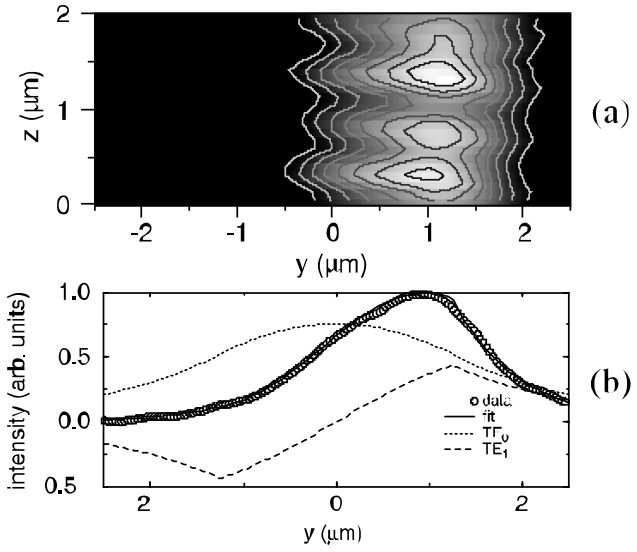

Fig 9: (a) Optical image obtained at the surface of the waveguide when TE modes are excited. A line-cut at y=1 μm exhibits mostly sinusoidal behavior, with a peak-to-valley ratio of 1.3. (b) Intensity line-cut taken at constant z, with a fit consisting of the weighted superposition of TE_0 (59%) and TE_1 (41%), with a phase difference of 0.098 radians. The theoretical solutions are also shown for TE_0 and TE_1.

For the intended waveguide design, we expect a similar behavior of the guided modes for TE polarization with only minor changes in the mode shapes and ***k*** values. However, a NSOM scan for TE in Fig. 9(a) is dramatically different: the peak intensity is strongly off-center,

indicating a contribution from a higher order mode. The design wavelength is very close to the cutoff condition of the first higher order mode, TE_1. A slight variation in physical parameters could cause the waveguide to become double moded. Since the modes have different field penetrations into the cladding, they have different values for n_{eff}, resulting in an accumulation of phase difference as they propagate. Therefore TE_0 and TE_1 beat against each other. A fit of an intensity line-cut taken at constant *z*, shown in Fig. 9(b), allows us to determine the phase and relative contributions of TE_0 and TE_1.

The simultaneous existence of TE_0 and TE_1, which propagate with different n_{eff} values, will cause beating in the standing modes, as shown in the data of Fig. 10. The period of this beating provides a direct measure of the modal index difference between these two guided modes:

$$T = \frac{\pi}{\left(k_z^{TE_0} - k_z^{TE_1}\right)} = \frac{\lambda_0}{\left(n_{eff}^{TE_0} - n_{eff}^{TE_1}\right)} = \frac{\lambda_0}{2\Delta n_{eff}} \quad (1)$$

For T=25μm, we get $\Delta n_{eff} = 0.031$. A few percent variation in the waveguide width is considered consistent with the fabrication accuracy. Within these tolerances, a perfect match between the simulations and measured Δn_{eff} is obtained.

Fig 9(b) shows a line cut along the *y*, with a fit to the lowest order solution. The parameters of this fit give k_y in different regions of the waveguide. This technique is also applied to the TM modes in Fig. 7(c), though what we are observing is actually an average value for k_y, since it is not possible to get full *y* dependence using this fitting technique.

Finally, we are able to also separate k_z values for TE_0 and TE_1 by making use of the weight ratios from Fig. 9(b), the Δn_{eff} from Eqn. (1), and an average standing mode period from Fig. 9, using the equations

$n_{eff,avg} = a n_{eff,TE_0} + b n_{eff,TE_1}$

$n_{eff,TE_0} = n_{eff,avg} + b\Delta n_{eff}$. The complete

$n_{eff,TE_1} = n_{eff,avg} - a\Delta n_{eff}$

vectoral solution is summarized in table 1.

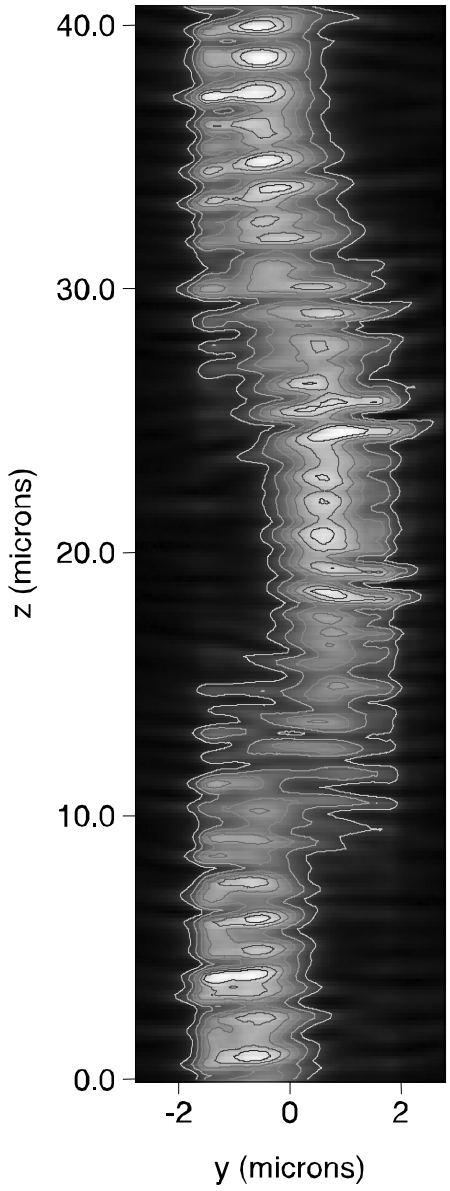

Fig 10 (left) Beating between the TE_0 and TE_1. The beat length can be measured to obtain a measure of Δn .

	α_x	k_y	k_z	n_{eff}
TE_0	4.615	0.645	6.110	1.506
TM_0	4.36	0.703	5.910	1.457
TE_1	4.313	0.783	5.869	1.447

Tab. 1: Measured wavevector components for the waveguide, shown in values of μm^{-1}.

STANDING MODE SPECTROSCOPY

Transmission measurements can provide information about overall cavity length, by looking at the free spectral range (FSR), or the distance between the peaks in transmission. The relationship is given by $FSR = \lambda^2 / 2n_{eff} d$ so that for a n_{eff} = 1.458, λ=1.549 μm, and *d* = 9mm (the measured distance between the entrance and exit facet), we get a FSR of 0.091nm. This is observed in a transmission spectrum. This measurement, while certainly useful, cannot determine the absolute position of a dielectric interface or a defect along the waveguide. We have developed a simple and direct measurement, called *standing mode spectroscopy*, which allows for identifying the precise location of any local interface. Fig. 10(a) shows the standing waves formed in the presence of a dielectric interface as a function of wavelength. Note that the slope of the lines formed by the standing waves as a function of the wavelength (λ) decreases for increasing distance from the fixed phase point at *z*=0, where the slope is infinite. The λ - dependence of the intensity at constant *z* provides information about the distance *d* of this measurement point to the output interface given by: $d = \pi\lambda_1\lambda_2 / 2(\lambda_1 - \lambda_2)$ To test the accuracy of this technique, we measure the standing mode in the waveguide as a function of wavelength in Fig. 10(b). Using the above analysis, we obtain a distance *d* of 5.19mm, correctly matching the distance from the probed region to the exit facet. This is an obvious result, but it should be understood that for more complex systems, which switch outputs or have complicated resonances, this technique could give a wealth of information about the various dielectric interfaces.

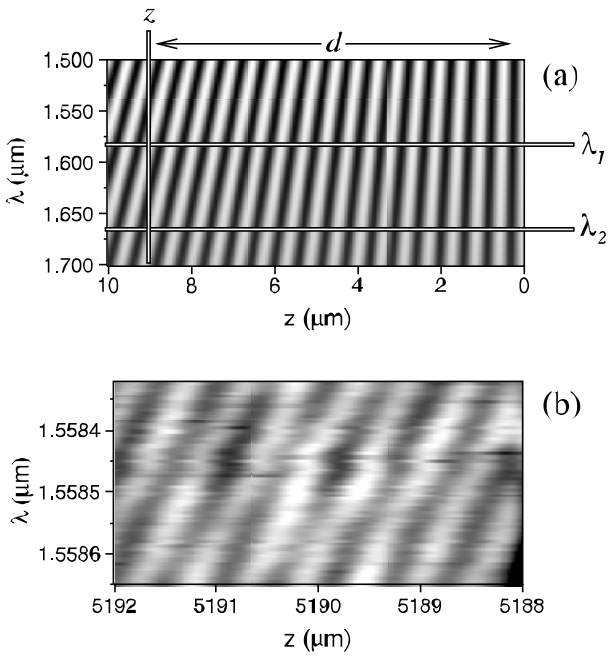

Fig 11 (a) Simulation of electric field intensity as a function of *z* and λ for a system with an interface at *z*=0 μm. The propagation direction is in the -*z* direction. Variables used to identify *d* are identified. (b) Experimental results for the waveguide. The interface is again at *z*=0.

PROBE PERTURBATION

A measurement technique should introduce negligible perturbation to the system under study. From our measurements of the optical modes on the surface, it is clear that this perturbation is small for the purposes of measuring k_z from the period of the standing mode.

The probe perturbation can evidence itself in two major ways. First, the presence of a scattering object (the NSOM probe) inside the evanescent field of the waveguide will take optical power out of the system, showing as a reduction in overall transmission through the waveguide. Second, the presence of an object above the waveguide will change the local index of refraction at that point above the waveguide. As we saw in the beginning of this chapter, this could cause the mode to be locally attracted to a higher index of refraction, or locally repelled from a lower index (or reflecting material, such as a conductor).

First, we expect the reduction in transmission due to scattering into the probe to be related to the nature of the probe used. For our experiments, we used two different types of probes: uncoated probes, and probes coated with ~100 nm of Al. We would expect the metal coated probe to have significantly more scattering, and thus significantly more reduction in transmission.

The amount of light detected by the tip as it is scanned across the waveguide is compared to the amount of light simultaneously transmitted through the waveguide in Fig. 11. In both the coated and uncoated cases, we see a slight drop in transmission that is correlated exactly to the light collected by the NSOM probe. As we expect, the reduction in transmission in the case of the coated probe is about double that in the case of the uncoated probe.

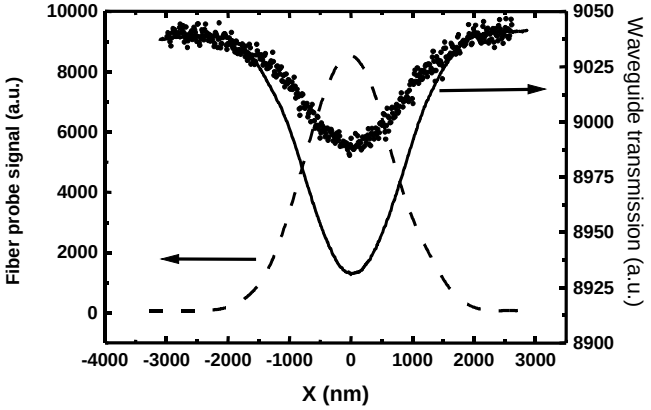

Fig 11: Signal collected by the NSOM probe (left scale, solid) and light transmitted through the waveguide for the coated probe (right scale, dashed) and the uncoated probe (right scale, circles) as a function of lateral distance across the waveguide. When the NSOM probe is collecting light, the transmitted signal is reduced at most by about 1\%.

The amount of reduction is between about 0.5% and 1.2%. Typical transmission values for pulled, coated tips such as these are between 10^{-4} and 10^{-6}, so it is within reason we would detect 1pW using an NSOM probe that is collecting 1% of the 10 μW launched into the waveguide.

MODE MOVEMENT

The second effect is that the position of the mode will move differently due to the change in the local index of refraction comparing the coated to uncoated probe case. We can see this by doing a simple two dimensional mode simulation for the system. The probe is modeled using a layer made up of two parts. The first, long part is the *a* layer of index *n*=1.44, simply pure silica. The second part is a varying thickness of either metal or of silica, depending on whether we are modeling a coated or uncoated probe. By varying the separation *d*, we are effectively varying the distance the probe is from the surface.

The effect of the NSOM probe is obtained by comparing the field intensities around the core peak for three different cases; the unperturbed case, the metal coated probe or uncoated probe. We find that the metal coated tip tends to repel the mode, while the uncoated tip tends to attract the mode.

It is not obvious what effect, if any, this mode movement will have on a measurement of the evanescent decay constant. To answer this question theoretically, we did multiple simulations of the system, varying the probe-to-sample spacing *d*. We assumed that the value measured by the probe will be proportional to the field intensity just outside the probe. Performing this simulated experiment, find that although the overall intensity is different, the decay constants are almost exactly the same: $2\alpha_x$ = 8.981 μm for the uncoated case, and $2\alpha_x$ = 9.001 μm for the coated case.

To test the validity of the simple simulations and our intuition, we repeated the vertical scan NSOM experiments using a coated probe (similar to Fig. 3). We obtained good exponential behavior over several orders of magnitude, measuring a decay constant of $2\alpha_x = 8.886\ \mu m$. This is slightly smaller than the decay constant measured using the coated probe, but only by about 1.2%. This confirms that while the coated probe scatters more radiation, the effect on the internal mode structure of the waveguide is minimal, yielding a nearly identical exponential decay constant, in agreement with our simple model.

From these measurements, it is clear that the perturbation due to the probe is small enough to perform basic measurements of propagation parameters. What is not clear is just how small the perturbation is. More detailed studies should be performed, utilizing measurement techniques with higher signal to noise, to determine exactly the scale of the perturbation. An interesting measurement would be to go over exactly the same point on the waveguide with a coated, then an uncoated probe. We might expect to see a narrower transverse mode profile due to the movement of the mode caused by the boundary condition imposed by the metal.

CONCLUSIONS

In this paper we have used near-field scanning optical microscopy to measure the internal spatial modes and complete local properties controlling optical wave propagation in glass/silica buried waveguides. We have shown that measurements of the period of the observed standing modes provides an accurate and direct measure of the effective index, which combined with the measured transverse modal shape and decay constants, determines the values of all spatial components of the wave vector. Standing mode spectroscopy is a new technique that can provide information about the locations of remote dielectric interfaces based upon the rate of change in the phase of the standing wave as a function of wavelength. Finally, experimental and theoretical results addressing the issue of perturbation of the NSOM probe on the measurement of the local field shows a weak but measurable perturbation. These results and measurement techniques can now be applied to more complex systems.

REFERENCES

1. K. J. Ebeling, *Integrated Optoelectronics*, Springer-Verlag, New York, (1993).
2. E. H. Synge, "A suggested method for extending microscopic resolution into the ultra-microscopic region," *Phil. Mag*., vol. 6, pp. 356--362, (1928).
3. D. W. Pohl, W. Denk, and M. Lanz, "Optical Stethoscopy: Image Recording with Resolution l/20," *Appl. Phys. Lett*., vol. 44, no. 7, pp. 651--653, (1984).
4. E. Betzig, A. Lewis, A. Harootunian, M. Isaacson, and E. Kratschmer, "Near-field Scanning Optical Microscopy (NSOM): Development and Biophysical Applications," *Biophys. J*., vol. 49, pp. 268--279, (1986).
5. L. McCaughan and E. E. Bergmann, "Index Distribution of Optical Waveguides from Their Mode Profile," *J. Lightwave Tech*., vol. 1, pp. 241, (1983).
6. G. N. van den Hoven, A. Polman, C. van Dam, J. W. M. van Uffelen, and M. K. Smit, "Direct imaging of optical interferences in erbium-dopedAl_2O_3 waveguides," *Optics Letters*, vol. 21, no. 8, pp. 576--579, 15 April 1996.
7. T. J. Rogers, D. G. Deppe, and B. G. Streetman, "Effect of an AlAs / GaAs mirror on the spontaneous emission of an InGaAs-GaAs quantum well," *Appl. Phys. Lett*., vol. 57, no. 18, pp. 1858--1860, 29 October 1990.

8. S. E. Burns, N. Pfeffer, J. Gruner, M. Remmers, T. Javorek, D. Neher, and R. H. Friend, "Measurements of optical electric field intensities in microcavities using thin emissive polymer films," *Adv. Mater.*, vol. 9, no. 5, pp. 395--405, April 1997.
9. D. P. Tsai, H. E. Jackson, R. C. Reddick, S. H. Sharp, and R. J. Warmack, "Photon scanning tunneling microscope study of optical waveguides," *Appl. Phys. Lett.*, vol. 56, no. 16, pp. 1515--1517, 16 April 1990.
10. P. L. Phillips, J. C. Knight, B. J. Mangan, P. St. J. Russell, M. D. B. Charlton, and G. J. Parker, "Near-field optical microscopy of thin photonic crystal films," *J. Appl. Phys.*, vol. 85, no. 9, pp. 6337--6342, 1 May 1999.
11. S. Bourzeix, J. M. Moison, F. Mignard, F. Barthe, A. C. Boccara, C. Licoppe, B. Mersali, M. Allovon, and A. Bruno, "Near-Field Optical Imaging of Light Propagation in Semiconductor Waveguide Structures," *Appl. Phys. Lett.*, vol. 73, no. 8, pp. 1035--1037, 24 August 1998.
12. P. K. Tien, J. P. Gordon, and R. Whinnery, "Light waves in thin films and integrated optics," *Proc. IEEE,* vol. 53, pp. 129, 1965.
13. G. H. Vander Rhodes, M. S. Unlu, B. B. Goldberg, J. M. Pomeroy, and T. F. Krauss, "Characterisation of Waveguide Microcavities using High-resolution Transmission Spectroscopy and Near-field Scanning Optical Microscopy," *IEE Proc. Optoelectron.*, vol. 37, no. 4, pp. 379—383, (1998).
14. B. E. Little, S. T. Chu, W. Pan, D. Ripin, T. Kaneko, Y. Kokubun, and E. P. Ippen, "Vertically Coupled Glass Microring Resonator Channel Dropping Filters," *Phot. Tech. Lett.*, vol. 11, no. 2, pp. 215--217, February 1999.
15. B. E. Little, J. S. Foresi, G. Steinmeyer, E. R. Thoen, S. T. Chu, H. A. Haus, E. P. Ippen, L. C. Kimerling, and W. Greene, "Ultra-Compact Si-SiO2 Microring Resonator Optical Channel Dropping Filters," *Phot. Tech. Lett.*, vol. 10, no. 4, pp. 549--551, April 1998.
16. K. Karrai and R. D. Grober, "Piezoelectric Tip-Sample Distance Control for Near Field Optical Microscopes," *Appl. Phys. Lett.*, vol. 66, no. 14, pp. 1842--1844, 1995.
17. E. A. J. Marcatelli, "Dielectric Rectangular Waveguide and Directional Coupler for Integrated Optics," *Bell Syst. Tech. J.*, vol. 48, pp. 2071--2102, 1969.
18. W. W. Lui, C. L. Xu, W. P. Huang, K. Yokoyama, and S. Seki, "Full-vectoral mode analysis with considerations of field singularities at corners of optical waveguides," *J. Lightwave Tech.*, vol. 17, no. 8, pp. 1509--1513, 1999.